A Supervised Bayesian Method for Cerebrovascular Segmentation

Jutao Hao, Minglu Li
Department of Computer Science and Engineering
Shanghai Jiaotong University
A0403321,800 Dongchuan Road, Min Hang,200240 Shanghai,
P.R. China
jutaohao@sjtu.edu.cn

Abstract: - In this paper, we present a supervised statistical-based cerebrovascular segmentation method from Time-Of-Flight MRA. The novelty of this method is that rather than model the dataset over the entire intensity range, we at first use a low threshold to eliminate the lowest intensity region, and then use two uniform distributions to model the middle and high intensity regions, respectively. Subsequently, in order to overcome the intensity overlap between subcutaneous fat and arteries, a high order multiscale features based energy function is introduced to enhance the segmentation. Comparing with those sole intensity based segmentation method the newly proposed algorithm can solve the problem of the regional intensity variation of TOF–MRA well and improve the quality of segmentation. The experimental results also show that the proposed method can provide a better quality segmentation than sole intensity information used method.

Key-Words: Statistical segmentation, Bayesian method, Maximum a posteriori (MAP) estimation, Markov Random field, High-order multiscale features.

1 Introduction

The human cerebrovascular system is a complex three-dimensional anatomical structure and a three-dimensional (3D) representation of vasculature can be extremely important in image-guided neurosurgery, pre-surgical planning and clinical analysis.

Magnetic resonance angiography (MRA) is a noninvasive medical imaging modality that produces three dimensional (3D) images of vessels and cavities. Three major groups of MRA techniques are time-of-flight (TOF) MRA, contrast enhanced (CE) MRA and phase contrast (PC) MRA. TOF exploits the difference in the amplitude of longitudinal magnetization between flowing and static spins. The TOF technique is not quantitative but it is widely used clinically because it is fast and provides high contrast images, which is the main motivation behind our study. Although its importance is well-known, a three-dimensional representation of blood vessels is not available directly. A common approach is to use a maximum intensity projection (MIP) where three-dimensional (3D) data is projected onto a 2D plane by choosing the maximal intensity value along that projection direction. However, a major drawback of this method is that the background artefacts and other tissues may occlude vascular structures of low contrast and small width. Thus, it is desirable to extract the vasculature tree before it is visualized.

A variety of the methods have been developed for extracting blood vessels [1,2] and all of these methods can be classified into three main categories: deformable model [3,4,5,6,7,8,], statistical models [9,10,11,12] and multiscale filtering [13,14,15,16].

Since statistically based parametric techniques are efficient and easy to implement，they have been widely used to classify vessels in magnetic resonance angiography. Several researchers have demonstrated that, with a proper statistical mixture model for the observed intensity distribution of an angiogram, the expectation maximization (EM) algorithm followed by an estimator can be used to segment vascular structures [9,10,12,17]. Model selection is an important issue in this kind of statistical segmentation techniques. According to the intensity range, three major classes can be found in a TOF MRA dataset: the lowest intensity region corresponds to cerebrospinal fluid (CSF), bone, and the background air. The middle intensity region corresponds to brain tissues, including both the grey and white matter, and parts of the eyes. The third high intensity region corresponds to subcutaneous fat and arteries.

In [9], a normal distribution is used to model each of the low and middle intensity regions, while a uniform distribution is used to model the vessels class as shown in Fig. 1(a). Chung et al. introduced a Rician distribution for background noise modelling [10]. Hassouna et al. found that Rayleigh

distribution provides an accurate fit when compared with the normal distribution, and use an additional normal distribution to describe the overlap the background and the brain tissues. And using a normal distribution instead of the uniform distribution describes the distribution of the blood vessels [12], the histogram and mixture fit are shown in Fig.1 (b).

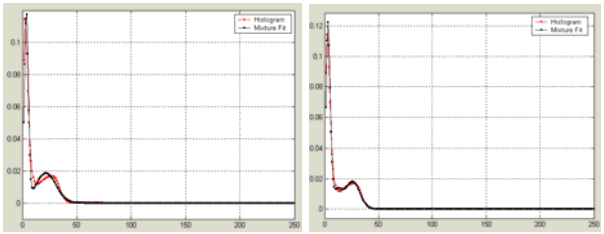

(a) (b)

Fig 1. (a) Model by Wilson and Noble (1999). (b) Model by Hassouna (2006)

To the best of our knowledge, in the literature, the researchers have been laying a strong emphasis on the model selection over the entire dataset and pursuing automatic segmentations. However, after inspecting over different TOF MRA datasets, we found that the distributions of the background and the overlap between background and the brain tissue are not always fitted very well. So, there is none a FMM can be applicable to all different clinical datasets. Furthermore, for the purpose of binary segmentation, there is not necessary to find a FMM over the entire dataset which is complex, time consuming and may not get an accurate segmentation. At the same time, due to the overlap between subcutaneous fat and arteries, certain postprocessings are indispensable for reclassifying them. Thus, such an automatic global thresholding is not automatic yet.

In our research, we at first use a low threshold to eliminate the lowest intensity region, and then use two uniform distributions to model the middle and high intensity regions, respectively. Subsequently, in order to reclassify the subcutaneous fat and arteries, a high order multiscale features based energy function is introduced into the Bayesian framework to get the complete cerebrovascular segmentation.

2 Problem Formulation

Traditional Markov random field (MRF) based segmentation algorithm requires modeling two random fields. Let $S = \{1,...,N\}$ where N is the total number of voxels. $X = (X_s)_{s \in S}$ is unobservable MRF, also called the label field and x is a realization of X. The image to be segmented y is a realization of the observed random field $Y = (Y_s)_{s \in S}$. Let $L = \{background, vessel\}$ and x be a binary segmentation of the image y, and then each element in the x can be regarded as a mapping from S to L. A feasible segmentation x is, therefore, in a Cartesian product Ω_x of label sets. The set Ω_x is known as the configuration space.

The process of segmentation is to find x^* which represents the correct tissue class at each voxel site given by image y. we attempt to find the MAP estimation from the MRA dataset.

$$x^* = \arg\max_{x \in \Omega_x} p(x \mid y) \tag{1}$$

where

$$p(x \mid y) = \frac{p(y \mid x)p(x)}{p(y)} \tag{2}$$

where $p(y \mid x)$ is the posterior probability of y conditioned on x, $p(x \mid y)$ denotes the probability distribution of x conditioned on y. $p(y)$ is a priori probability of y, and $p(x)$ is the probability distribution of x. Because the prior probability of image p(y) is independent of the segmentation x, so above equation can be rewritten as

$$p(x \mid y) \propto p(x, y) = p(x)p(y \mid x) \tag{3}$$

The likelihood and the prior probabilities are also known as the observation and the prior models in the Bayesian segmentation framework.

2.1 Observation Model

In practice, due to high complexity of the random variables X and Y, an assumption is made that intensity values in the image are independent and identically distributed, and can be modeled by a FMM[[18].

For every $l \in L$ and $s \in S$

$$p(X_s = l) = \omega_l \tag{4}$$

is independent of the individual sites $s \in S$ and ω_l ($l \in L$) called mixing parameter. We take Φ as the model parameter set with

$$\Phi = \{\omega_l; \theta_l \mid l \in L\} \tag{5}$$

Consider two configuration x and y. The joint probability distribution of x and y dependent on the model parameters can be written as

$$\begin{aligned} p(x, y \mid \Phi) &= \prod_{s \in S} p(y_s, x_s \mid \Phi) \\ &= \prod_{s \in S} \{\omega_l f(y_i; \theta_{x_i})\} \end{aligned} \tag{6}$$

we can compute the marginal distribution of y dependent on the parameter set Φ

$$p(y|\Phi)=\sum_{l\in L}p(l,y|\Phi)=\prod_{s\in S}\omega_l\cdot f(y;\theta_l) \quad (7)$$

This is the so-called finite mixture model (FMM).

In this section, we first use a low threshold to eliminate the low intensity region, and then use two normal distributions to fit the rest histogram. The histogram of the processed dataset and the mixture fit are shown in Fig.2. Thus, the mixture distribution of two Gaussian distributions is defined by

$$f(x)=\sum_{l=1}^{2}\omega_l f_l(x). \quad (8)$$

where the function $f_l(x)$ $l=[1,2]$ are the normal density functions. The quantities ω_1 and ω_2 are the class proportions which sum is unity.

$$f_l(x)=\frac{1}{\sqrt{2\pi}\sigma_l}\exp(\frac{-(y-\mu_l)^2}{2\sigma_l^2}) \quad l=[1,2] \quad (9)$$

Expectation Maximization (EM) can be used to estimate the parameters of a chosen distribution for a set of data by maximizing the likelihood of the distribution [19]. In the EM algorithm the distribution parameters are iteratively estimated by updating initial parameter estimates under the constraint that the difference between the log-likelihoods of the mixture distribution is to be minimized.

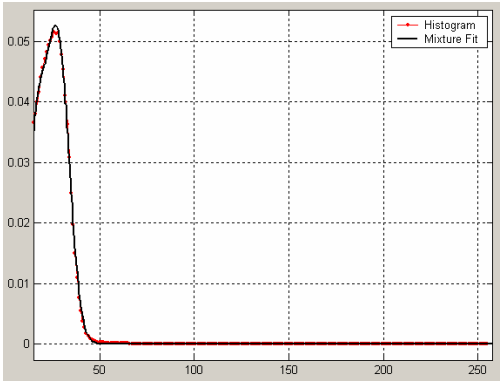

Fig. 2 Histogram and Mixture fit of processed dataset.

2.2 Prior Model

The spatial property can be modelled through different aspects, amongst which the contextual constraint is a general and powerful one. MRF theory provides a convenient and consistent way to model context-dependent entities such as image pixels and correlated features.

An MRF is characterized by its local property (the Markovianity) whereas a GRF is characterized by its global property (the Gibbs distribution). The Hammersley-Clifford theorem [20] establishes the equivalence of these two types of properties. The theorem states that X is an MRF on S with respect to N if and only if X is a GRF on S with respect to N. Hence, if X is a MRF, its joint probability can be given by

$$\mathrm{P(X=x)}=\frac{1}{Z}e^{-\frac{U(x)}{T}} \quad (10)$$

where

$$Z=\sum_{x\in\Omega_X}e^{-\frac{1}{T}U(x)} \quad (11)$$

is a normalizing constant called the partition function, T is a constant called the temperature which shall be assumed to 1 unless otherwise stated, and $U(x)$ is the energy function. The energy

$$U(x)=\sum_{c\in C}V_c(x) \quad (12)$$

is a sum of clique potentials $V_c(x)$ over all possible cliques C. The value of $V_c(x)$ depends on the local configuration on the clique c.

In this paper, isotropic Multi-level Logistic (MLL) Model is adopted as MRF model and only pair-wise cliques are considered. The potential function for pair-wise cliques is written as

$$U(x_s)=\sum_{r\in\eta_s}V(x_s,x_r) \quad (13)$$

where η_s is the neighbourhood of s and the potential functions are defined as

$$V(x_s,x_r)=\begin{cases}-\beta_{sr} & x_s=x_r\\ +\beta_{sr} & x_s\neq x_r\end{cases} \quad (14)$$

The parameter β_{sr} describes the strength of the interaction between pair-wise neighbouring voxels.

Classification of the blood vessels is equivalent to find the optimal labelling using the maximum a posteriori (MAP) estimator:

$$x^*=\arg\min_{x\in\Omega_x}(U(y|x)+U(x)) \quad (15)$$

where $U(y|x)=-\log p(y|x)$ represents the likelihood energy function and $U(x)=\sum_{c\in C}V_C(x)$ is the prior energy function.

Although this type of statistically based parametric techniques have been widely used to classify vessels in

magnetic resonance angiography (MRA) and gotten a great success. There are still some misclassified voxels because of the overlap between background and arteries. For example, some vessel voxels may be classified as non-vessel class in regions with significant vascular signal loss due to complicated flow conditions including slowly and turbulent blood flow. On the other hand, some background voxels may be classified as blood vessels class, when the noise has high intensity value.

However, a spatial representation of small vessels and their branches which exhibit much variability are most important in planning and performing neurosurgical procedures. The more minute the information is, the more precise the navigation and localization of computer guided procedures. Present representations do not yield this kind of information. A more precise spatial representation of this complex anatomic structure is needed.

In the first step of classification, the two functions $U(y \mid x)$ and $U(x)$ are not sufficient to reclassify the tiny vessels and high intensity background noise because of the intensity overlap between them. It is, therefore, necessary to introduce other information to deal with this problem. In fact, the high-order differential image information provides a rich description of the brain tissue and blood vessels in the medical imagery and therefore we have added a third term into the energy function, which is obtained by high order information analysis.

The speed image of TOF MRA provides information of the patients' blood flow. The intensity values in the image are proportional to the flow velocity. Because of the blood viscosity, frictional force slows down the blood flow near the vascular wall. As such, the intensity profile is nonuniform within the vascular structures. Analyzing the intensity values distribution of structures in TOF MRA, images within a local neighborhood play an important role. Many different techniques have been proposed for analysis the local structure of the image [3, 6, 7, 8]. The differential invariants constitute a complete and irreducible set of differential operators appropriate for the description of the local image structure up to any desired order.

For a point *s* in the image, a feature vector $f(s)$ is assigned

$$f(s) = (f_{\sigma 0}, \ldots f_{\sigma n})(s) \tag{16}$$

where each $f_{\sigma n}$ is the vector of differential invariants computed at scale σ_n.

$$f_{\sigma n}(s) = (I_{1\sigma n}, I_{2\sigma n}, \lambda_{1\sigma n}, \lambda_{2\sigma n}, \lambda_{3\sigma n}, R_A, R_B, S) \tag{17}$$

$$R_A = \frac{|\lambda_{2\sigma n}|}{|\lambda_{3\sigma n}|} \tag{18}$$

$$R_B = \frac{|\lambda_{1\sigma n}|}{\sqrt{|\lambda_{2\sigma n}\lambda_{3\sigma n}|}} \tag{19}$$

$$S = \sqrt{\lambda_{1\sigma n}^2 + \lambda_{2\sigma n}^2 + \lambda_{3\sigma n}^2} \tag{20}$$

where $I_{1\sigma}$ and $I_{2\sigma n}$ represent the fist and second order Gaussian derivatives computed at scale σ_n .The parameters $\lambda_{1\sigma n}$, $\lambda_{2\sigma n}$ and $\lambda_{3\sigma n}$ represent the eigenvalues of the Hessian matrix of the image *I*, ordered by increasing magnitude. R_A differentiates between plate and line like structures, R_B accounts for deviation from a blob like structure, and S differentiates between vessel and background

Once the vector of differential invariants is computed on each voxel, the K-nearest neighbor algorithm (KNN) can be used to estimate the probability function for a voxel to belong to a class. In pattern recognition, kNN is a method for classifying objects based on closest training examples in the feature space. Thus, the probability for a voxel x to belong to a class C_i is computed for the formula

$$P(s \in C_i \mid f(s)) = \frac{\sum_{\bar{s} \in L_i \cap N_K(x)} \delta(f(s), f(\bar{s}))}{\sum_{\bar{s} \in N_K(s)} \delta(f(s), f(\bar{s}))} \tag{21}$$

where δ represents the Euclidean distance. $N_K(s)$ is the K nearest neighbours and L_i is the set of voxels of the training set that belongs to the class C_i. For blood vessel segmentation application C_0 and C_1 stand for background and blood vessels, respectively.

In general, the selection of the candidates for training is of great importance in the learning stage of any supervised pattern recognition method and the overall performance of the method strongly depends on the selection of these candidates. In our application, there are only two types of training points, namely, background (including of brain tissues and subcutaneous fat) and blood vessels. TOF MRA images have large regional variations in intensity and the thin blood vessels have low contrast between vessels and the background. Furthermore, in some case, aneurysm may be occurred. Hence, when we select the training points for blood vessels, all of the above conditions should be considered. After selected, the corresponding feature vectors are computed and stored.

By now, high-order multiscale features based energy function can be defined as:

$$U(p(s \in C_0 \mid f(s))) = \begin{cases} \lambda \times p(s \in C_0 \mid f(s)) \\ \quad if\ p(s \in C_0 \mid f(s)) > 0.5\ and\ x_s = background \\ \lambda \times (1 - p(s \in C_0 \mid f(s))) \\ \quad if\ p(s \in C_0 \mid f(s)) < 0.5\ and\ x_s = vessels \end{cases} \tag{22}$$

where λ is a positive weighted coefficient.

Optimal labeling of the MRA data is obtained through the condition

$$x^* = \arg\min_{x \in \Omega_x} (U(y \mid x) + U(x) + U(p(s \in C_0 \mid f(s)) \tag{23}$$

The deterministic relaxation iterated conditional modes (ICM) is used for the MAP estimation [21]. Although the ICM usually converges to a local minimum of the energy function, this loss of optimality may be compensated for by an appropriated initial guess. In our experiments, we use maximum likelihood (ML) estimate [22]. The initial binary segmentation x^0 is obtained as follows:

$$x^0 = \{\arg\max_{x_s \in L} p(y_s \mid x_s \mid \forall s \in S)\} \tag{24}$$

3 Parameters Estimation

The mixture-density parameter estimation problem is probably one of the most widely used applications of the EM algorithm in the computational pattern recognition community, where the distribution parameters are iteratively estimated by updating initial parameter estimates under the constraint that the difference between the log-likelihoods of the mixture distribution is to be minimized. By minimizing that difference, the equations become:

$$\mu_l^{new} = \frac{\sum_{s \in S} p^{old}(l \mid y_s) y_s}{\sum_{s \in S} p^{old}(l \mid y_s)} \tag{25}$$

$$(\sigma_l^{new})^2 = \frac{\sum_{s \in S} p^{old}(l \mid y_s)(y_s - \mu_l^{new})^2}{\sum_{s \in S} p^{old}(l \mid y_s)} \tag{26}$$

$$\omega_l^{new} = \frac{1}{N} \sum_{s \in S} p^{old}(l \mid y_s) y_s \tag{27}$$

where N is the total number of voxels being considered and y_s is the intensity of voxel at location s. The function $p^{old}(l \mid y_s)$ is the conditional probability of voxel s belonging to class l at current iteration and is defined as

$$p^{old}(l \mid y_s) = \frac{\omega_l p^{old}(y_s \mid l)}{\sum_{j=0}^{j=2} \omega_j p^{old}(y_s \mid j)} \tag{28}$$

The common approach is to run the EM algorithm more than once, starting from different sets of initial parameter values and then selecting the estimated set and maximizing the conditional expectation, which is computationally expensive and the convergence is still not guaranteed. In this research, we adopt a histogram analysis based initialization method to find a good initial estimate to above parameters.

On the other hand, in the MRF prior model, there are two free parameters, β_{sr} and λ. There are several MRF parameter estimation techniques such as the coding method [23], the least square error method [24] and the maximum pseudo likelihood estimator (MPLE) method. In this work, the MRF parameters are found empirically. The sensitivity of the MRF parameters in the segmentation is analyzed. In order to find the optimal parameters, we have tested each combination of parameters by changing β_{sr} from zero to 1 with an incremental step of 0.1 and λ from zero to 10 with an incremental set of 1.

4 Experimental Results

Since a complete vasculature is very complex, the manual segmentation by experts is unavailable. Therefore, in order to validate our method, we applied our algorithm to synthetic 3D volume with data volume 256x256x9 voxels. Furthermore, our algorithm has also been exerted on several real clinical datasets.

To compromise between the computational speed and the accuracy of the algorithm, in the following experiments, only three different scales have been used, namely, $\sigma_0 = 0.8$, $\sigma_1 = 2$ and $\sigma_2 = 4$,which cover most of the objects from the thinnest arteries of interest to the thickest arteries in the datasets. In each experiment, 100 points have been selected for vessels and backgrounds.The number of the nearest neighbors is set as $K = 10$.

4.1 Synthetic Image Volume

In this experiment, a synthetic image volume containing several blood vessels was built. A slice of the volume is shown in Fig. 3(a). All the blood vessels are generated using a parabolic intensity

profile and 8 voxels width. The noisy image with SNR= 4 and its truth segmentation is presented in Fig. 3(b) and (c), respectively. Fig. 3(d) gives the probability image derived from Equ(21). The segmentation results using sole intensity information and both information are illustrate in Fig. 3(e) and (f). A quantitative analysis of misclassified error for each slice in the volume is illustrated in Fig.3 (g). The misclassified error of our method and intensity information alone is 3.32947% and 4.38046%, respectively. Notice that all segmentation results in this experiment are obtained without spatial contextual information.

The segmentation error is calculated by counting the number of misclassified voxels, which is given by

$$Error = \frac{\text{Number of misclassified voxels}}{\text{Total number of voxels in the image}} \times 100\% \quad (29)$$

4.2 Clinical Data Sets

In order to evaluate performance of our algorithm, we have tested our algorithm on several 3D TOF clinical datasets. For real clinical images, a quantitative assessment is very difficult because the complete vasculature is very complex and the manual segmentation by experts is unavailable. Even the manually-obtained segmentations cannot be considered "ground truth" since many vessels is not obtained and bright areas not corresponding to vessel are included in some cases. In the following experiments, qualitative comparisons are shown only due to the difficulty of obtaining ground truth segmentations for datasets.

To show the accuracy of the segmentation, a comparison is done with the maximum intensity projection (MIP) [25] and Hassouna's method [12], which is a recent unsupervised sole intensity based segmentation algorithm for blood vessel segmentation.

The first dataset used here was acquired on a 1.5T scanner with voxel size of 0.859×0.859×1.017 mm^3 and image size of 256x256x115 voxels.

In Fig.4, the influence of parameter λ has been tested. From (c) to (g) we can find that with the increment of λ more and more high intensity backgrounds such as eye and subcutaneous fat are eliminated f the segmentation results. Fig.4 (b) and (c) give the segmentation results using Hassouna's method and our proposed preprocessing based two-Gaussian mixture model. Note that the noise in Fig.4. (b) is not filtered using largest connected components. Segmentation result using proposed method is shown in Fig. 5 from different viewpoints.

To validate our algorithm, the algorithm has been exerted on another two clinical datasets. The data volume in the second dataset is 256 ×256 ×79 voxels with a voxel size of 0.938 ×0.938 ×2 mm^3. The second dataset contains 256 ×256 ×129 voxels and with a voxel size of 0.859×0.859×1mm^3.

In the following two experiments, the parameter configurations were: $\beta_{sr} = 0.5$ and $\lambda = 5$. MIP images, segmentation results using Hassouna's method (without postprocessing) and our proposed method are present in Fig 6 (a), (b) and (c), respectively.

5 Conclusion

In this paper, we have introduced a Bayesian image segmentation method for cerebrovascular segmentation from TOF MRA. The novelty of this method is that rather than relying on the intensity feature alone, high-order feature is used to enhance the segmentation result. In particular, the use of high order multiscale information provides a richer description of the different tissues in medical imagery than the description solely provided by the intensity distributions.

In order to evaluate the algorithm, the proposed methodology has been applied to both the synthetic and real clinical image volumes. In synthetic image experiment, the segmentations produced by the newly proposed algorithm are in high degree of agreement with the ground truth. However, due to the complexity of the whole cerebrovascular tree, the ground truth is unavailable by manual segmentation. To compensate for the loss of ground truth, we have compared our algorithm with both MIP and Hassouna's method [12]. The comparison results illustrate that the proposed method can provide a better quality segmentation than sole intensity information used method.

References:

[1] Suri J.S., Liu K., Reden L., Laxminarayan S., A review on MR vascular image processing: skeleton versus nonskeleton approaches: part II. IEEE Transactions on Information Technology in Biomedicine . 2002, 6 (4), 338–350.

[2] Kirbas C., Quek F., A review of vessel extraction techniques and algorithms. Tech. rep., VisLab Wright State University, Dayton, OH, USA, Nov. 2002.

[3] Kass M., Witkin A., Terzopoulos D., Snakes: Active contour models. International Journal of Computer Vision. 1987,1 (4), 321–331.

[4] Lorigo L.M., Faugeras O.D., Grimson W.E.L., et al.,. CURVES: curve evolution for vessel segmentation. Med. Image, 2001, Anal. 5, 195–206.
[5] Wink, O., Niessen, W.J., et al., Fast delineation and visualization of vessels in 3-D angiographic images. IEEE Trans. Med. Imaging. 2000, 19 (4), 337–346.
[6] Deschamps, T., Cohen, L.D., Fast extraction of tubular and tree 3D surfaces with front propagation methods. In: Proceedings of the 16th ICPR, 2002, 731–734.
[7] Yan, Pingkun; Kassim, Ashraf A., Segmentation of volumetric MRA images by using capillary active contour. Medical Image Analysis 2006 pp. 317-329
[8] Hernandez, M., Frangi, A.F., Non-parametric Geodesic Active Regions: Method and evaluation for cerebral aneurysms segmentation in 3DRA and CTA, Medical Image Analysis (2007), doi: 10.1016/ j.media.2007.01.002.
[9] Wilson D.L., Noble J.A , An adaptive segmentation algorithm for time-of-flight MRA data. IEEE Trans. Medical Imaging, 1999,18(10), 938—945.
[10] Chung, A.C.S., Noble, J.A.: Statistical 3D vessel segmentation using a Rician distribution. MICCAI'99 (1999) 82-89.
[11] Chung, A.C.S., Noble, J.A., Summers, P., Fusing speed and phase information for vascular segmentation of phase contrast MR angiograms. Med. Image Anal. 2002, 6 (2), 109–128.
[12] Hassouna, A.A. Farag, S. Hushek, and T. Moriarty, Cerebrovascular Segmentation. from TOF Using Stochastic Models, Medical Image Analysis,2006, Vol 10, pp. 2-18.
[13] Sato, Y., Nakajima, S., Shiraga, N., Atsumi, H., Yoshida, S., Koller, T., Gerig, G., Kikinis, R., Three-dimensional multi-scale line filter for segmentation and visualization of curvilinear structures in medical images. Medical Image Analysis 1998, 2(2), 143–168.
[14] Krissian, K., Malandain, G., Ayache, N., Model based detection of tubular structures in 3D images. INRIA Technical Report 373, 1999.
[15] Frangi, A.F., Niessen, W.J., Vincken, K.L., Viergever, M.A., Multiscale vessel enhancement filtering. Proc. Int'l Conf. Medical Image Computing Computer- Assisted Intervention. Lect. Notes Comp. Sci. 1998, 130–137.
[16] Lorenz, C., Carlsen, I.-C., Buzug, T.M., Fassnacht, C., Weese, J., 1997. A multi-scale line filter with automatic scale selection based on the Hessian matrix for medical image segmentation. Proc. Scale-Space Theories in Computer Vision. Lect. Notes Comp. Sci. 1997 (1252), 152–163.
[17] Ayman El-Baz, Aly A. Farag, Georgy L. Gimel'farb, Stephen G. Hushek: Automatic Cerebrovascular Segmentation by Accurate Probabilistic Modeling of TOF-MRA Images. MICCAI 2005: 34-42.
[18] McLachlan J., Peel D., Finite Mixture Models. New York: Wiley,2000.
[19] Dempster A. P., Laird N. M., and Rubin D. B. ,Maximum likelihood from incomplete data via the EM algorithm J. R. Statist. Soc. B, vol. B39, no. 1, pp. 1–38, 1977.
[20] Geman S., Geman D., Stochastic relaxation, Gibbs distributions,and the Bayesian restoration of images, IEEE Trans. Pattern Anal. Machine Intell.1984, 6,721–741.
[21] Besag, J., On the statistical analysis of dirty pictures. J. Roy. Statist. Soc., 1986, Ser. B 48, 259–302.
[22] Li S. Z., Markov Random Field Modeling in Image Analysis, 2nd ed. Tokyo, Japan: Springer-Verlag, 2001.
[23] Besag, J., Spatial interaction and the statistical analysis of lattice systems. J. Roy. Statist. Soc., 1974.,Ser. B 36, 192–236.
[24] Derin, H., Elliott, H.,. Modeling and segmentation of noisy and textured images using Gibbs random fields. IEEE Trans. Pattern Anal. Machine Intell. 1987, 9 (1), 39–55.
[25] Rossnick, S., Laub, G., Braeckle, G., Bachus, R., Kennedy, D., Nelson, A., Dzik, S., Starewicz, P.,Three dimensional display of blood vessels in MRI. In: Proceedings of the Computers in Cardiology, 1986, 193–196.

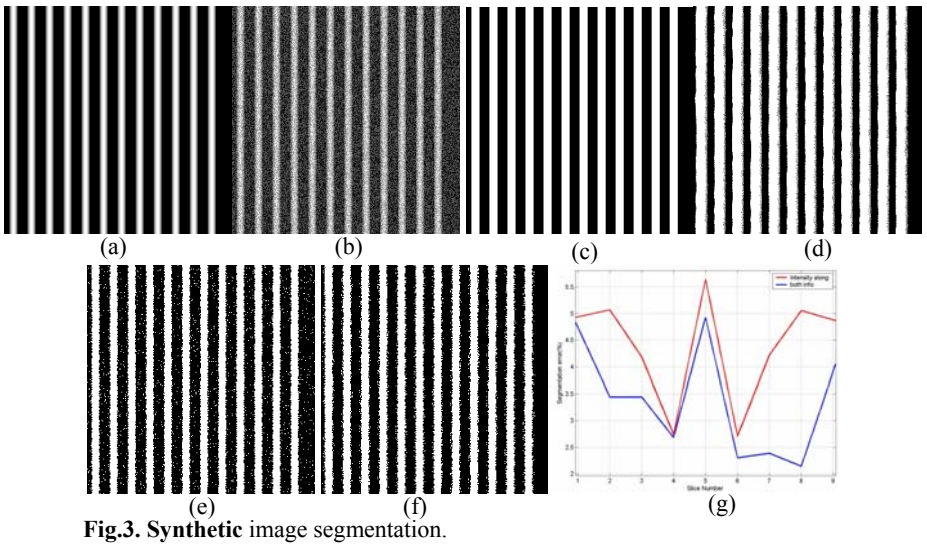

Fig.3. Synthetic image segmentation.
(a)A middle slice of synthetic volume.(b)Noisy image with SNR=4;(c)Ground truth
(d) Probability for tube. (e). Segmented image using intensity information alone.
(f) Segmented image using intensity and high order multiacle information.
(g) Segmentation error on each slice.

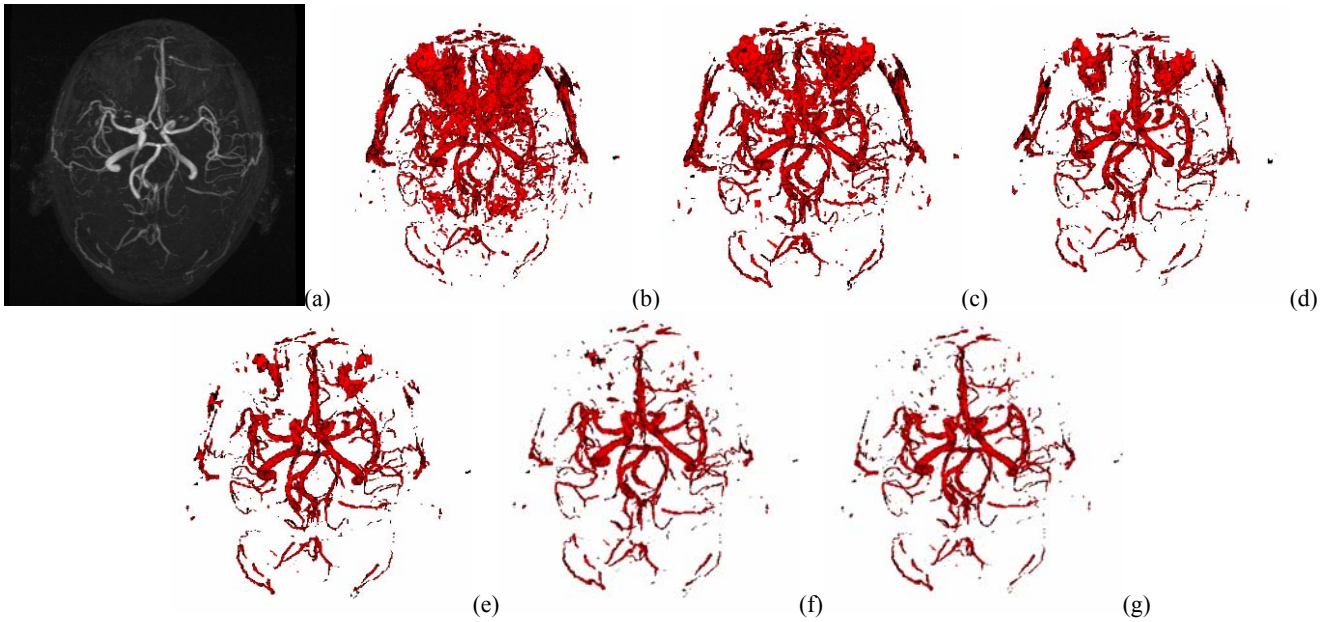

Fig. 4 (a) MIP image; (b) Segmentation using Hassouna's method;(c) Segmentation result using two Gaussian model.; From (c) to (g) Three-dimensional surfaces of the segmentation results with parameter $\lambda = 0$, $\lambda = 2$, $\lambda = 5$, $\lambda = 8$ and $\lambda = 10$,respectively.

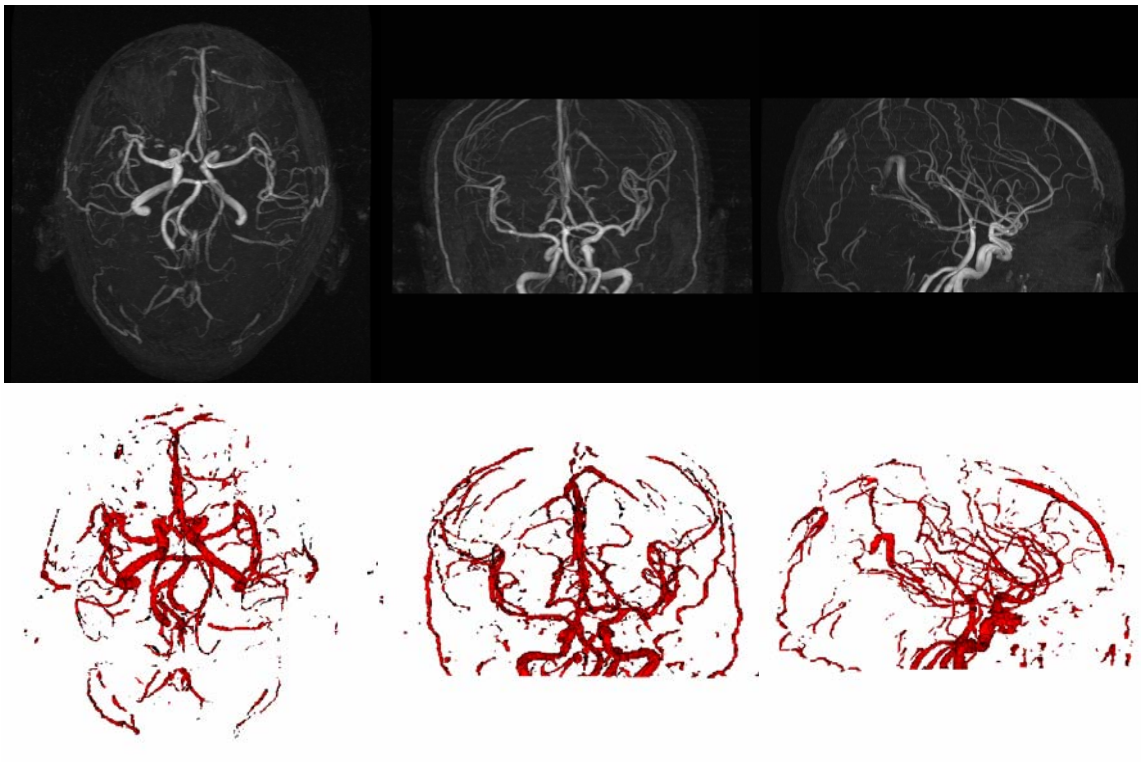

Fig.5. Segmentation result using proposed method is shown from different viewpoints.

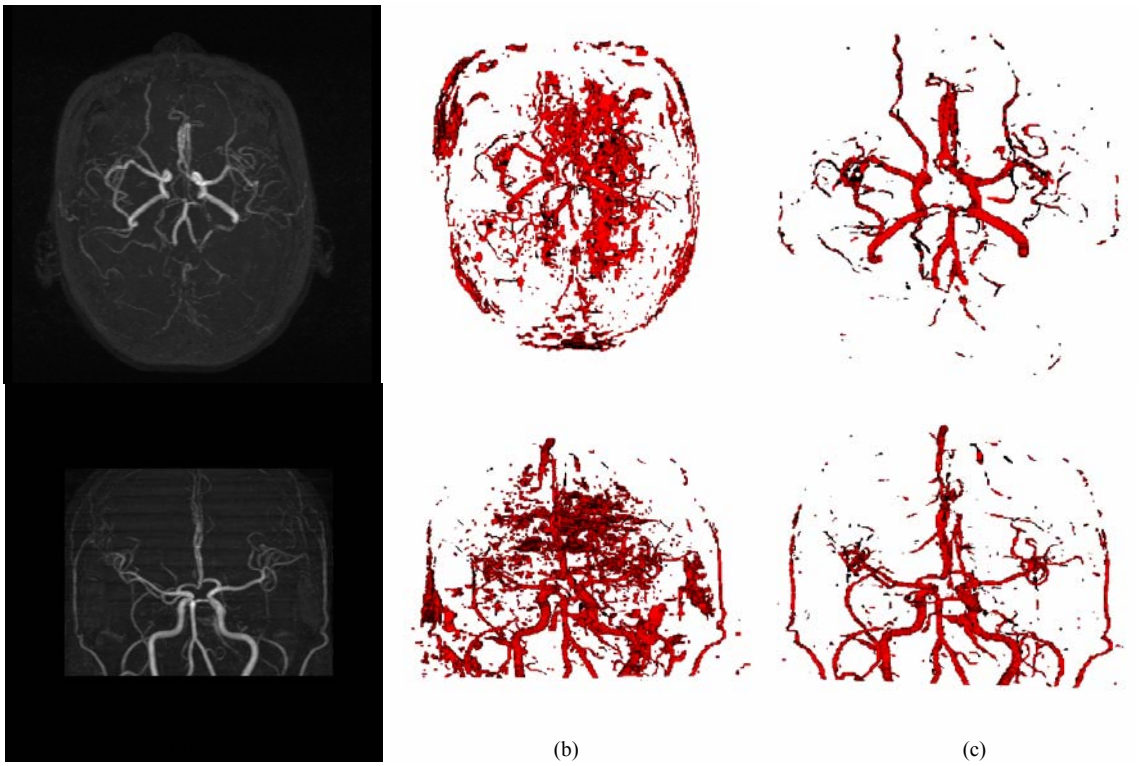

Fig.6. Comparison of segmentation results .(a) MIP; (b) Segmentation result using Hassouna's method; (c) Segmentation result using our method.